

‘Jet breaks’ and ‘missing breaks’ in the X-Ray afterglow of Gamma Ray Bursts

Shlomo Dado¹, Arnon Dar² and A. De Rújula³

ABSTRACT

The X-ray afterglows (AGs) of Gamma-Ray Bursts (GRBs) and X-Ray Flashes (XRFs) have, after the fast decline phase of their prompt emission, a temporal behaviour varying between two extremes. A large fraction of these AGs has a ‘canonical’ light curve which, after an initial shallow-decay ‘plateau’ phase, ‘breaks smoothly’ into a fast power-law decline. Very energetic GRBs, contrariwise, appear not to have a ‘break’, their AG declines like a power law from the start of the observations. Breaks and ‘missing breaks’ are intimately related to the geometry and deceleration of the jets responsible for GRBs. In the frame of the ‘cannonball’ (CB) model of GRBs and XRFs, we analyze the cited extreme behaviours (canonical and pure power law) and intermediate cases spanning the observed range of X-ray AG shapes. We show that the entire panoply of X-ray light-curve shapes –measured with Swift and other satellites– are as anticipated in the CB model. We test the expected correlations between the AG’s shape and the peak- and isotropic energies of the prompt radiation, strengthening a simple conclusion of the analysis of AG shapes: in energetic GRBs the break is not truly ‘missing’, it is hidden under the tail of the prompt emission, or it occurs too early to be recorded. We also verify that the spectral index of the unabsorbed AGs and the temporal index of their late power-law decline differ by half a unit, as predicted.

¹dado@phep3.technion.ac.il

Physics Department and Space Research Institute, Technion, Haifa 32000, Israel

²arnon@physics.technion.ac.il; arnon.dar@cern.ch

Physics Department and Space Research Institute, Technion, Haifa 32000, Israel
Theory Unit, CERN, 1211 Geneva 23, Switzerland

³alvaro.derujula@cern.ch

Theory Unit, CERN, 1211 Geneva 23, Switzerland and
Physics Department, Boston University, USA

1. Introduction and résumé

The isotropic distribution of gamma ray bursts (GRBs) in the sky and their number distribution as function of intensity, measured with the BATSE instrument aboard the Compton Gamma Ray Observatory, provided the first observational evidence that gamma ray bursts (GRBs) originate at large cosmological distances (Meegan et al. 1992). Moreover, the rapid variation of their light curves (Bahat et al. 1992) indicated that their huge energy is emitted from a very small volume. In the original fireball (FB) model of GRBs (e.g. Paczynski 1986; Goodman 1986; Rees & Mészáros 1992) the emission was spherically symmetric. The implied isotropic energy release of GRBs in γ -rays often exceeded $M_{\odot} c^2$, creating an ‘energy crisis’. Indeed, such a mighty, abrupt, compact, and γ -ray-efficient source was unforeseen.

A simple solution to this puzzle was suggested by Shaviv and Dar (1995): the γ -ray emission is narrowly collimated by the relativistic motion of their *jetted* source, which is seen when it points closely enough to the observer. In this view, GRBs are not produced by fireballs, but by inverse Compton scattering of light by highly relativistic jets of ordinary matter, ejected in violent stellar processes such as supernova explosions, mergers of neutron stars (Paczynski 1986; Goodman, Dar & Nussinov 1987; Dar et al. 1992), or the direct collapse of massive stars to black holes without a supernova (Woosley 1993).

The sky localization of GRBs by BeppoSAX (Costa et al. 1997) led to the discovery (Groot et al. 1997; van Paradijs et al. 1997) of their optical afterglows (AGs) and their host galaxies (Sahu et al. 1997) which were used to extract their cosmological redshifts (Metzger et al. 1997). The AGs seemed to follow an achromatic power-law decline, as expected from a highly relativistic expanding fireball that drives a blast wave into the circumburst environment (e.g., Mészáros & Rees 1997). This prediction of the spherical fireball model (see e.g., Piran 1999) being independent of the assumption of spherical symmetry, it was also argued that the AGs, like the GRBs themselves, are produced by narrowly collimated jets (Dar 1997, 1998).

The concept of jets was incorporated into the FB model by the substitution of its spherical shells by conical sections thereof, the mechanism for the γ -ray emission still being synchrotron radiation from shock-accelerated $e^+ e^-$ pairs in a baryon-poor material (see, e.g. Piran 1999, 2000; Mészáros 2002 and references therein), in spite of the difficulties that such a radiation mechanism encounters (Ghisellini et al. 2000).

An elegant and simple way to distinguish between a conical jet and a spherical fireball was suggested by Rhoads (1997): the AG of a decelerating conical jet will show an achromatic steepening –a *jet break*– in its power-law decline when the relativistic beaming angle of its radiation becomes larger than the opening angle of the jet. Soon afterwards, better sampled

data on the optical afterglow of GRBs showed the existence of what appeared to be such achromatic jet breaks (Harrison et al. 1999; Stanek et al. 1999), and the spherical FB model was modified into a *collimated fireball* model (e.g. Piran, Sari & Halpern 1999). In this model GRB pulses are produced by synchrotron radiation from the collision between conical sections of shells. The collision of the ensemble of shells with the interstellar matter (ISM) generates the AG by synchrotron radiation from the forward shock propagating in the ISM, and/or from the backwards shock within the merged shells. Rhoads (1999) and Sari, Piran and Halpern (1999) derived a relation between the opening angle of the conical jet and the time of the jet break. This relation has been applied extensively to the pre-Swift data to infer the opening angle of the conical jet and to determine the ‘true’ energy of GRBs, posited to be an approximate standard candle (Frail et al. 2001).

Since the launch of Swift the above generally-accepted ‘standard’ paradigm has been challenged, due to the absence of breaks in the AGs of many GRBs (Panaitescu et al. 2006; Burrows and Racusin 2006), to the chromatic behaviour of the AG of other GRBs having the alleged ‘jet break’ (Stanek et al. 1999, Harrison et al. 1999), and to the failure of the Frail relation (Frail et al. 2001) in many Swift GRBs (Kocevski & Butler 2007). In the fireball model, the jet breaks need not be sharp; they are often parametrized with a varying smoothness (Stanek et al. 1999). Allowing for such breaks, Covino et al. (2006) could not identify a Swift GRB with a fully achromatic break. Liang et al. (2007) have extended this study, and analyzed the Swift X-ray data for the 179 GRBs detected between January 2005 and January 2007 and the optical AGs of 57 pre- and post-Swift GRBs. They found that not a single burst satisfies all the criteria of a jet break. This brings us fully into the question of the nature and properties of the jets responsible for GRBs and their AGs and, more specifically in this paper, to the understanding of ‘breaks’ and ‘missing breaks’.

An alternative to the fireball scenario is offered by the ‘cannonball’ (CB) model of GRBs [Dar & De Rújula 2000a, 2004, hereafter DD2000a, 2004; Dado, Dar & De Rújula (hereafter DDD) 2002; for a recent review see De Rújula 2007]. In this model *long-duration* GRBs and their AGs are produced by bipolar jets of CBs (Shaviv & Dar 1995; Dar & Plaga 1999), ejected in *ordinary core-collapse* supernova (SN) explosions as matter is accreted onto the newly-formed compact object (De Rújula 1987). The ‘cannon-balls’ are made of *ordinary-matter plasma*. The γ -rays of a single pulse of a GRB are produced as a CB coasts through the SN *glory*—the initial SN light, scattered away from the radial direction by the ‘wind’: the ejecta puffed by the progenitor star in a succession of pre-SN flares. The electrons enclosed in the CB raise the glory’s photons to GRB energies by *inverse Compton scattering (ICS)*. As a CB coasts through the glory, the distribution of the glory’s light becomes increasingly radial and its density decreases rapidly. Consequently, the energy of the up-scattered photons is continuously shifted to lower energies and their number decreases swiftly, resulting in a fast

softening and decline of the prompt emission (DD2004, 2007a,b). In the CB model, the AG of a GRB is due to *synchrotron radiation (SR)* from swept-in ISM electrons spiraling in the CB’s enclosed turbulent magnetic field, generated by the intercepted ISM nuclei and electrons (DDD2002). At X-ray energies, the SR afterglow begins to dominate the ICS prompt emission only during the fast-decline phase of the latter (DDD2006).

In the CB model, the *beau rôle* in the understanding of GRBs is played by the Doppler factor, $\delta(t)$, relating times, energies and fluxes in a CB’s rest system to those in the observer’s system. Its form in terms of the observer’s angle θ (relative to the CB’s direction of motion) and the time-dependent Lorentz factor, $\gamma(t)$, of a CB, is:

$$\delta(t) = \frac{1}{\gamma(t) [1 - \beta(t) \cos \theta]} \approx \frac{2\gamma(t)}{1 + [\gamma(t) \theta]^2}, \quad (1)$$

where the approximation is excellent for $\gamma \gg 1$ and $\theta \ll 1$. The decrease of $\gamma(t)$ with time, as a CB encounters the particles of the ISM, is calculable on grounds of energy-momentum conservation (DDD2002, Dar & De Rújula 2006, thereafter DD2006). The energy-integrated energy flux of the AG of a GRB, is $\propto \delta^3$. Let $\gamma_0 \equiv \gamma(0)$. Consider a CB that is observed almost on axis, so that $\theta \gamma_0 < 1$: the observer is *ab initio* within the opening cone of the relativistically beamed radiation. As $\gamma(t)$ decreases, $\delta(t)$ monotonically decreases and so does the observed AG. Consider the same CB, viewed by an observer at a much larger angle, so that $\theta \gamma_0$ is ‘a few’. As $\gamma(t)$ decreases, $\delta(t)$ in Eq. (1) *increases*, reflecting the fact that the characteristic opening angle of the radiation, $1/\gamma(t)$, is reaching the observer’s direction. Past the point $\gamma \theta \sim 1$, the decrease of $\delta(t)$ is monotonic, as in the first case we considered. The AG radiation parallels again the behaviour of $\delta(t)$. For observers of the same GRB from different angles, as θ increases at fixed $\gamma(t)$, the AG’s flux decreases. All these simple facts, supported by the corresponding explicit derivations, are reflected in Fig. 1a, which we have copied from DDD2002, as it foretells the progressive variety of AG shapes to be studied here.

There is more to Fig. 1a than what we said. The Lorentz factor $\gamma(t)$ of a CB only begins to change significantly, in a calculable manner, when the increase in its mass –induced by the energy influx of the swept-in ISM particles– becomes comparable to the CB’s initial mass. This happens, as we shall review, at a time $t_b \propto [1 + 2\theta^2 \gamma_0^2]/\gamma_0^3$. At fixed $\gamma(t)$, as reflected in Fig. 1a, a larger θ entails a larger t_b . This achromatic ‘deceleration bend’ at $t = t_b$, we believe, was often interpreted in FB models as a putative jet break.

Naturally, the values of γ_0 and δ_0 of a given CB also affect the properties of its prompt ICS-dominated radiation (we are presenting this introductory discussion as if there was a single CB generating the prompt and AG radiations, a simplification to be undone when needed). In the CB model the ICS-dictated (θ, γ_0) dependences of a CB’s isotropic energy, peak energy and peak luminosity are $E_{\text{iso}} \propto \delta_0^3$, $E_p \propto \gamma_0 \delta_0$ and $L_p \propto \delta_0^4$ (DD2000b). The

conditions for these quantities to be relatively large (a relatively small θ or a large γ_0) are the ones leading to a luminous AG with a small t_b . The basis for one of these expected correlations, studied before in detail in DDD2007c, is illustrated in Fig. 1b.

If the deceleration bend at time t_b takes place *after* the fast-decline phase of the prompt emission, it is observable, and the unabsorbed X-ray light curve is canonical (DDD2002). In these cases, there is a ‘break’. If t_b takes place earlier, it is hidden under the prompt emission, and only the tail of the canonical behaviour, namely the ‘late’ power-law decline of the unabsorbed synchrotron afterglow, is observable. In these cases, the break is missing. The transition from long-plateau, clearly ‘broken’ AGs, to power-law like ‘unbroken’ AGs should be anticorrelated with the trend from under-‘energetic’ to over-energetic GRBs.

In the CB model the late-time spectral energy density F_ν of the X-ray and optical AG tends to a time and energy-dependence $\propto t^{-(p+1)/2} \nu^{-p/2}$, with p the spectral index of the electrons accelerated within a CB and cooled by the emission of the very SR seen as the AG. A prediction that we have not emphasized before is that the temporal power decline should be, GRB by GRB, half a unit steeper than the spectral decline.

In DDD2006, 2007a we have demonstrated that the most common light curves of the X-ray AG of GRBs are well described by the CB model. We have also explained there the various origins of the chromatic behaviours of AGs. In DDD2007b we have focused on the fast decline phase of the prompt emission and we have demonstrated that the rapid spectral evolution observed during this phase is also as expected in the CB model. In DDD2007c we have shown, for large ensembles of GRBs, how the observed correlations between E_{iso} , E_p [Dar & De Rújula 2000b (DD2000b), Amati et al. 2002], L_p , and other prompt observables (pulse rise-time, lag-time and variability) follow mainly from the same simple geometrical considerations –that we have reviewed above– on the case-by-case variability of the Doppler factor. In the CB model, XRFs are simply GRBs seen at relatively large θ (DDD2004a), even the particularly interesting XRF 060218 is in no way exceptional (DDD2007a).

In this paper we focus on the shape of the light curves of the X-ray afterglow of GRBs, with and without breaks, measured with the X-ray telescope (XRT) aboard Swift. We show that the shapes of the X-ray light curves of GRBs and XRFs predicted in Fig. 1a, and the correlation between t_b and E_{iso} illustrated Fig. 1b (and the consequent apparent presence or absence of breaks in the AG) agree with the CB-model’s expectations. We also analyze the (t_b, E_p) correlation on the same light. Finally, we investigate the relation between the temporal power-law index of the post-break decline and the photon spectral index, reaching satisfactory results. To do all this, we investigate 16 GRBs chosen to reflect the full span of the question of the presence or absence of breaks. The selected GRBs range from the faintest known GRB (980425, of supernova-association fame), which also has the most pronounced

plateau and the latest break time, to the brightest Swift GRB (061007), with the most luminous and longest-observed unbroken power-law X-ray AG.

2. The afterglow of a decelerating CB

In the CB model, the mechanism for the emission of the prompt radiation of GRBs and XRFs is inverse Compton scattering. The temporal and spectral properties of the prompt phase, including its fast decline, are summarized in a ‘master formula’ (DD2004) that we have already contrasted with Swift data (DDD2006, 2007a,b,c,d). We shall not repeat it here—as our emphasis in the current study is on breaks in the X-ray light curves of GRB afterglows—though we shall use it to describe the fading of the prompt emission until the take-over by the synchrotron-AG emission, and the occasional late X-ray flares. Neither do we discuss here the optical AGs (DDD2007a). The extinction in the optical- and, more so, in the radio- domain (within the CBs, in the circumburst environment, in the ISM of the host galaxy and ours, and in the intergalactic medium) are difficult to model as reliably as the X-ray extinction. We shall see once again that the X-ray light curves (corrected for extinction) carry clear and direct information on the radiation mechanisms that dominate the prompt emission and the AG phase (ICS and SR, respectively, in the CB model).

During the initial phase of γ -ray emission in a GRB, the Lorentz factor γ of a CB stays put at its initial value $\gamma_0 = \mathcal{O}(10^3)$, for the deceleration induced by the interactions with the ISM has not yet had a significant effect. The Doppler factor by which the light emitted by a CB is boosted in energy is given by Eq. (1). Since the emitted light is forward-collimated into a cone of characteristic opening angle $1/\gamma$, the boosted energetic radiation is easiest to detect for $\theta = \mathcal{O}(1/\gamma_0)$. Thus, typically, $\delta_0 = \mathcal{O}(10^3)$.

As a CB ploughs through the ISM, fully ionized by the preceding γ radiation, it gathers and scatters the ISM ions, mainly protons. These encounters are ‘collisionless’ since, at about the time it becomes transparent to radiation, a CB also becomes ‘transparent’ to hadronic interactions. As a consequence of momentum conservation, the scattered and re-emitted protons inevitably exert an inwards ‘pressure’ on the CB. We have assumed that the main effect of this pressure is to slow the CB’s expansion, posited to be relativistic at the emission time. In the approximation of isotropic re-emission in the CB’s rest frame and a constant ISM density n , one then finds that, typically within minutes of observer’s time t , a CB reaches a roughly ‘coasting’ radius, $R = \mathcal{O}(10^{14} \text{ cm})$, which increases slowly until the CB finally stops and blows up (DD2006). Up to the end of the coasting phase, and in a constant density ISM, $\gamma(t)$ obeys (DDD2002):

$$(\gamma_0/\gamma)^{3+\kappa} + (3 - \kappa) \theta^2 \gamma_0^2 (\gamma_0/\gamma)^{1+\kappa} = 1 + (3 - \kappa) \theta^2 \gamma_0^2 + t/t_0,$$

$$t_0 = \frac{(1+z) N_B}{(6+2\kappa) c n \pi R^2 \gamma_0^3}, \quad (2)$$

where $\kappa=1$ if the ISM particles re-emitted fast by the CB are a small fraction of the flux of the intercepted ones. In the opposite limit, $\kappa=0$. In the CB model of cosmic rays (DD2006), the observed spectrum strongly favours $\kappa=1$, used here in our fits. We have also concluded from previous analysis of Swift X-ray data that $\kappa \approx 1$ is the right choice.

As indicated by first-principle calculations of the relativistic merger of two plasmas (Frederiksen et al. 2004), the ISM ions continuously impinging on a CB generate within it turbulent magnetic fields, which we assume to be in approximate energy equipartition with the energy of the intercepted ISM, $B \approx \sqrt{2 \pi n m_p c^2} \gamma$. In this field, the intercepted electrons emit synchrotron radiation. The SR, isotropic in the CB’s rest frame, has a characteristic frequency, $\nu_b(t)$, the typical frequency radiated by the electrons that enter a CB at time t with a relative Lorentz factor $\gamma(t)$. In the observer’s frame:

$$\nu_b(t) \simeq \frac{\nu_0}{1+z} \frac{[\gamma(t)]^3 \delta(t)}{10^{12}} \left[\frac{n}{10^{-1} \text{ cm}^3} \right]^{1/2} \text{ Hz}. \quad (3)$$

where $\nu_0 \sim 8.5 \times 10^{16} \text{ Hz} \simeq 354 \text{ eV}$. The spectral energy density of the SR from a single CB at a luminosity distance D_L is given by (DDD2003a):

$$F_\nu \simeq \frac{\eta \pi R^2 n m_e c^3 \gamma(t)^2 \delta(t)^4 A(\nu, t)}{4 \pi D_L^2 \nu_b(t)} \frac{p-2}{p-1} \left[\frac{\nu}{\nu_b(t)} \right]^{-1/2} \left[1 + \frac{\nu}{\nu_b(t)} \right]^{-(p-1)/2}, \quad (4)$$

where $p \sim 2.2$ is the typical spectral index⁴ of the Fermi accelerated electrons, $\eta \approx 1$ is the fraction of the impinging ISM electron energy that is synchrotron re-radiated by the CB, and $A(\nu, t)$ is the attenuation of photons of observed frequency ν along the line of sight through the CB, the host galaxy (HG), the intergalactic medium (IGM) and the Milky Way (MW):

$$A(\nu, t) = \exp[-\tau_\nu(\text{CB}) - \tau_\nu(\text{HG}) - \tau_\nu(\text{IGM}) - \tau_\nu(\text{MW})]. \quad (5)$$

The opacity $\tau_\nu(\text{CB})$ at very early times, during the fast-expansion phase of the CB, may strongly depend on time and frequency. The opacity of the circumburst medium [$\tau_\nu(\text{HG})$ at early times] is affected by the GRB and could also be t - and ν -dependent. The opacities $\tau_\nu(\text{HG})$ and $\tau_\nu(\text{IGM})$ should be functions of t and ν , for the line of sight to the CBs varies

⁴The normalization in Eq. (3) is only correct for $p > 2$, for otherwise the norm diverges. The cutoffs for the ν distribution are time-dependent, dictated by the acceleration and SR times of electrons and their ‘Larmor’ limit. The discussion of these processes being complex (DDD2003a, DD2006), we shall satisfy ourselves here with the statement that for $p \leq 2$ the AG’s normalization is not predicted.

during the AG observations, due to the hyperluminal motion of CBs. These facts, the different (t, ν) dependences of the ICS and SR emissions, and the dependence of the synchrotron AG on $\nu_b(t)$, are responsible for the complex observed chromatic behaviour of the AGs. To a fair approximation, though, the deceleration bend, if occurring late enough, is achromatic from X-ray energies to the optical domain (DDD2002) but not as far as radio (DDD2003a).

The Swift X-ray bands are above the characteristic frequency ν_b in Eq. (3) at all times. It then follows from Eq. (4) that the *unabsorbed* X-ray spectral energy density has the form:

$$F_\nu \propto R^2 n^{(p+2)/4} \gamma^{(3p-2)/2} \delta^{(p+6)/2} \nu^{-p/2} = R^2 n^{\Gamma/2} \gamma^{3\Gamma-4} \delta^{\Gamma+2} \nu^{-\Gamma+1}, \quad (6)$$

where we have used the customary notation $dN_\gamma/dE \approx E^{-\Gamma}$.

3. Breaks, missing breaks, and the AG's asymptotic power decline

The functions $\delta(t)/\delta_0$ and $\gamma(t)/\gamma_0$ of Eqs. (1,2) evolve slowly, up until a time:

$$\begin{aligned} t_b &= [1 + 2\theta^2 \gamma_0^2] t_0 \\ &\approx (130 \text{ s}) [1 + 2\gamma_0^2 \theta^2] (1+z) \left[\frac{\gamma_0}{10^3} \right]^{-3} \left[\frac{n}{10^{-1} \text{ cm}^{-3}} \right]^{-1} \left[\frac{R}{10^{14} \text{ cm}} \right]^{-2} \left[\frac{N_B}{10^{50}} \right], \end{aligned} \quad (7)$$

where we scaled the result to typical CB-model values of R and a CB's baryon number, N_B . The combination of the parameters n , R and N_B appearing in Eq. (7) is best constrained by the excellent X-ray observations discussed here. Our previous results on optical and radio AGs (for fixed R and N_B) favoured 10 times a smaller n at the much larger sampled times, not an inconsistency, since a CB travels for $\sim \gamma \delta$ light-days in one day of GRB data. We have chosen to normalize n as in Eq. (7), rather than to reproduce long discussions on the distributions of CB-model parameters (e.g. De Rújula 2007).

The quantity t_b in Eq. (7) characterizes the *deceleration bend-time* of the CB model; Eq. (2) for $\gamma(t, t_0, \theta, \gamma_0)$ describes the gradual character of this 'break'. At later times Eq. (2) implies that $\gamma \rightarrow \gamma_0 (t/t_0)^{-1/4}$, and Eq. (1) that $\delta \rightarrow 2\gamma$. Thus, at $t \gg t_b$, Eq. (6) yields:

$$\begin{aligned} F_\nu(t) &\propto t^{-1/2-p/2} \nu^{-p/2} = t^{-\Gamma+1/2} \nu^{-\Gamma+1}, \\ p &= 2(\Gamma - 1) \end{aligned} \quad (8)$$

with, as announced, a power decay in time half a unit steeper than in frequency.

4. The prompt observables

In the CB model, the peak energy of GRBs satisfies:

$$E_p \simeq \frac{1}{2} \frac{\gamma_0 \delta_0}{1+z} \epsilon_g, \quad (9)$$

where $\epsilon_g \sim 1$ eV is the typical energy of the glory’s photons, that of the associated-supernova early light just prior to the ejection of CBs. The isotropic (or spherical equivalent) energy of a GRB is (DD2004):

$$\begin{aligned} E_{\text{iso}} &\simeq \frac{\delta_0^3 L_{\text{SN}} N_{\text{CB}} \beta_s}{6c} \sqrt{\frac{\sigma_{\text{T}} N_{\text{CB}}}{4\pi}} \sim (1.2 \times 10^{53} \text{ erg}) V_E, \\ V_E &\equiv \frac{\delta_0^3}{10^9} \frac{L_{\text{SN}}}{L_{\text{SN}}^{\text{bw}}} \frac{N_{\text{CB}}}{2} \beta_s \sqrt{\frac{N_{\text{CB}}}{10^{50}}}, \end{aligned} \quad (10)$$

where L_{SN} is the mean supernova early optical luminosity, N_{CB} is the number of CBs in the jet, β_s is the comoving early expansion velocity of a CB (in units of $c/\sqrt{3}$), and σ_{T} is the Thomson cross section. For $\langle N_{\text{CB}} \rangle = 6$ (Schaefer 2007), the early SN luminosity required to produce the mean isotropic energy, $E_{\text{iso}} \sim 4 \times 10^{53}$ erg, of ordinary long GRBs, is $L_{\text{SN}}^{\text{bw}} \simeq 5 \times 10^{42}$ erg s⁻¹, the estimated early luminosity of SN1998bw. All quantities in Eq. (10) are normalized to their typical CB-model values. We have normalized to $N_{\text{CB}} = 2$, an adequate mean number of prominent X-ray pulses in the subset of GRBs analyzed here.

The results in Eqs. (9,10) are based on the assumption that ICS is the mechanism generating the prompt radiation. They depend on γ_0 and δ_0 , two parameters also appearing in the description of the SR afterglow. That is why we shall be able to test the implied correlations, GRB by GRB, between the shape of the AG and the energetics of the prompt radiation, the very strong dependence of the δ on θ playing once more the major role.

According to Eqs. (1,9,10), CBs with large γ_0 , and, more so, small θ , produce the largest values of E_p and E_{iso} : they generate the brightest GRBs. According to Eq. (7), such (γ_0, θ) values entail a small t_b , an expectation that our analysis will validate. In such cases the deceleration bend or ‘break’ of the synchrotron AG may take place before the beginning of the XRT observations and/or be hidden under the prompt Compton emission. According to Eq. (6), these AGs must be very luminous at early times, and according to Eq. (8), they must be well approximated from starters by the asymptotic power law behaviour given by Eq. (8). Our analysis will verify all these predictions.

5. Comparison with observations

To date, Swift has detected and localized nearly 300 long GRBs, and for most of them it followed their X-ray emission until it faded into the background. Incapable of discussing all of them, we analyze the light curves of the X-ray afterglow of a set of GRBs with and ‘without’ jet breaks, which represent fairly well the entire spectrum of canonical and non-canonical X-ray afterglows of GRBs. They include the most extreme cases of canonical and non canonical behaviour (GRB 0980425 and GRB 061126, respectively), the longest-measured canonical and non canonical X-ray light curves (GRB 060729 and GRB 061007) and a variety of light curves with and without breaks, with and without superimposed X-ray flares. Since many CB-model fits to canonical light curves of X-ray afterglows with ‘breaks’ were included in previous publications (DDD2002, 2006, 2007a,b,d) we shall discuss in this paper more cases of GRBs with an approximate power-law AG than of GRBs with a canonical AG.

We start the fits to the X-ray light curves during the transition between the rapid decline phase of the ICS-dominated prompt emission to the SR-dominated AG phase. It suffices to include the ICS contribution of the last prompt-emission pulse (or the last two), because of an exponential factor in the pulse shape that suppresses very fast the relative contribution of the earlier pulses by the time the data sample the later ones (DDD2007a,b). For the synchrotron contribution, it usually suffices to consider a common emission angle θ and an average initial Lorentz factor γ_0 for the ensemble of CBs. The ISM density along the CBs’ trajectories is approximated by a constant. We then fit the entire observations of the X-ray AG of the selected GRBs by using the ‘master formula’ [DD2004, Eq. (11) of DDD2007a], for the tail of the ICS prompt emission contribution, and Eq. (6) for the SR. Many GRBs have late X-ray flares, which we interpret as dying pangs of the engine, that is, the emission of CBs in late episodes of accretion into the recently collapsed central compact object. These CBs, whose ICS-generated flares can only be seen on the weak background of a decaying SR ‘after’-glow (quote-unquote, since the ‘AG’ is observable *before* the late ‘prompt’ flares), are also modeled with the same master formula.

The calculated shape of the energy-integrated X-ray AG, Eq. (6), depends only on three fit parameters. Two of them are the product $\gamma_0 \theta$ and the deceleration-bend time, t_b , for an on-axis observer, as given in the first line of Eq. (2). They determine the deceleration-bend time, t_b , observed at a viewing angle θ , see Eq. (7). The third fit parameter is the index p in the γ and δ time-dependent factors of Eq. (6). Unlike in previous analysis, we let p be a free parameter, unrelated to the spectral index Γ , independently extracted by the observers from the shape of the X-ray spectrum. This way we shall be able to test explicitly the CB-model prediction implied by Eq. (6), $p = 2(\Gamma - 1)$, or by its more readable asymptotic form, Eq. (8). In all the cases we study, but two (GRBs 071020 and 050416A), a single CB

or an ‘average’ CB suffice to describe the AG. The occasional need for two CBs in the AG light-curve description is not a novelty. The most notable instance is that of GRB 030329 (DDD2003b).

A comparison between the observed and predicted light curves of the 16 selected GRBs is shown in Figs. 2 to 5. When well-measured, the ‘break’ time, t_b , is indicated in the figure by an arrow. The best fit values, of p , $\gamma_0 \theta$, and t_b are listed in Table 1, along with additional observational information on these GRBs (redshift, peak energy, equivalent isotropic energy, the start-time of the Swift XRT observations, the spectral index of the unabsorbed AG, and the χ^2 per degree of freedom of the fits).

Afterglows which exhibit nearly a pure power-law decline, have a t_b smaller than t_s , the time after trigger when the XRT started its observations of the AG, or a t_b smaller than the time when the afterglow became brighter than the tail of the prompt emission. Such AGs have a nearly power-law shape, $F_\nu \sim t^{-p/2}$. Their fits, however, return upper limits for $\gamma_0 \theta$ and t_b , above which the shape of the AG deviates from the data. These limiting values are also reported in Table 1, but the corresponding limit- t_b location will not be shown in the figures in the case-by-case analysis, as it generally falls off-limits.

In most cases (including many Swift AGs studied in DDD2006, 2007a,b, but not shown here), the CB model produces good fits with reduced χ^2 values close to unity. Even if the χ^2 figures are good, we generally have refrained in the past from reporting them. One reason is that it is easy to obtain an excellent χ^2 for a fit that has many data points, but misses some that clearly reflect a significant structure (such as a supernova, see DDD2002), or is, even within errors, systematically above the data in one region and below it in another. For that reason, and the occasional local scatter of the data, we consider the eye to be a better judge than any statistical measure. We comment on the χ^2 values when they are ‘bad’.

The values of $\theta \gamma_0$, t_b (or t_0), and p returned by our fits and reported in Table 1 have formal errors of a few percent. The error-correlation matrix has relatively small off-diagonal elements. The reduced- χ^2 values are very close to unity, once the occasional flares are taken into account, to reveal the presence of a smoother SR background. One reason for all this is that t_0 sets the overall time scale, $\theta \gamma_0$ determines the shape of the bend, and p is sensitive to the whole SR light curve, playing a major role in its power-law tail. This means that when a light curve is well sampled (over orders of magnitude in flux and time), the fit is very sensitive to its parameters. Naturally, the results depend also on the deceleration law, Eq. (2), meant to be an approximation. Therefore the extracted parameters have ‘systematic’ errors reflecting the approximate nature of Eq. (2). We can argue explicitly why the approximation should be better than it looks at first sight, even case by case (on average, and independently, it leads to the correct spectrum of cosmic rays from non-relativistic energies up to the ‘knee’

at some 2×10^6 GeV, DD2006). The continuation of this rather formal argument on errors would take us well beyond the scope of this paper.

Case studies

In this section we comment one by one on the 16 GRBs or XRFs whose X-ray light curves we discuss. The results of the CB-model fits are shown in Figs. 2 to 5, and the parameters relevant to our discussion are listed in Table 1. The first eight GRBs are shown in the order of decreasing t_b . For the next four, only an upper limit on t_b can be extracted from the fits. The last four have very complex AGs.

The presence or absence of visible breaks in X-ray light curves and their different ‘look’ –the panoply of possibilities that we illustrate with our GRB choices– depend not only on t_b , but on its value relative to t_s (the start-time of XRT observations) and relative to the duration of the initial period of prompt-radiation dominance over the synchrotron AG. For this reason, it is easier to compare the plethora of looks of our GRBs in an order slightly different from that of a decreasing t_b . This we do (only) in the next paragraph.

GRBs 980425 and 060729 have light curves with a complete and simple canonical shape: one or two very clear prompt X-ray flares, a pronounced fast decay, a long plateau, a very visible ‘break’ smoothly bending at t_b to become a power-law decay. In GRBs 050401, 060105, 060418, 061007 and 050717, the plateau is becoming less and less pronounced, so that the AG’s t_b is hiding better and better under the prompt signal, to the point that the last two are close to a pure power-law tail. In GRBs 060813, 070508 and 050505, the prompt radiation ended early enough not to be caught by Swift’s XRT (in the last case the follow-up started very late), but this trio displays very canonical AGs, with their neat plateaus softly bending into a late power law. GRBs 071025, 061126 and 070125 are again approximate power-law tails, in which neither the early X-ray flares nor the putative bend are seen. GRBs 071020, 050416A and certainly 060607A, are very complex. The first two require contributions to the AG from two distinct CBs, 050416A having also a late flare. The unsightly X-ray light curve of GRB 060607A can be described by the CB model without any new ingredients, but not much is learned from fitting it.

GRB 980425. The light curve of this memorable single-peak GRB, as observed by BeppoSAX (Pian et al. 2000), is shown in Fig. 2a. The dotted line is the fit in DDD2002, showing what we called a pronounced ‘plateau’. We have added to it the last (predicted) data point, measured with Chandra by Kouveliotou et al. (2004), some 1285 days after burst! To be consistent with the analysis here, we have re-fit the ensemble of data in the same manner as

for all the other GRBs to be discussed. The result is the continuous curve in the figure. This GRB has, so far, the record large values $\gamma_0 \theta \approx 9.2$ and $t_b \approx 1.4 \times 10^5$ s, resulting in a light curve that rises before it falls, as explained in the introduction and illustrated in Fig. 1a. This is the behaviour expected for far-off-axis GRBs (DD2000a). This one barely missed the official classification as an XRF: it's E_p is ~ 56 keV, as opposed to $E_p < 50$ keV (see Dado & Dar 2005 for further comment on this point).

GRB 060729 and its X-ray light curve were studied in detail by Grupe et al. (2007). It has a canonical shape, the longest follow-up observations with Swift XRT, and the record-high $t_b \sim 8300$ s, among the Swift GRBs. In Fig. 2b we show its CB-model description with, superimposed on its prompt decline phase, four ICS X-ray flares included in the fit, as discussed in detail in DDD2007a. This GRB being ‘canonical’ and having a very clear ‘break’ –as several others also discussed in DDD2007a– is included here to illustrate the start of the transition from ‘breaks’ to ‘missing breaks’. Although the best fit to the X-ray AG appears to be excellent, it yields a large $\chi^2/dof = 635/140 = 4.5$, mostly due to many far-flung isolated data points in the Swift data. More accurate data from XMM Newton (Grupe et al. 2007) do not show such outliers. Eliminating their contribution yields the χ^2 value reported in Table 1.

GRB 050505, whose X-ray light curve was studied in detail by Hurkett et al. (2006). At $z=4.27$, this GRB is amongst the most distant with a known redshift. Due to an Earth-limb constraint, Swift was unable to slew to it until 47 minutes after the GRB’s trigger, and started measuring its X-ray light curve only 2883s after burst, during the transition of the AG from its shallow-decline phase to a power-law decline. As can be seen from Fig. 2c, the CB model describes very well the XRT light curve, except when the counting rate becomes comparable to the background.

GRB 050401, whose X-ray light curve, studied in detail by De Pasquale et al. (2006), evolves smoothly from the tail of the prompt emission at around 200s to a short decaying plateau, which suavely breaks into a power-law decline at $t \sim 2000$ s. Its CB-model description is shown in Fig. 2d. This GRB had a very bright X-ray AG, even though it originated at a fairly large redshift, $z=2.9$, and had a very large extragalactic absorbing column density along its sight-line, inferred from its X-ray spectrum to be $N = 1.7 \times 10^{22} \text{ cm}^{-2}$ (De Pasquale et al. 2006), or $N = 4 \times 10^{22} \text{ cm}^{-2}$ (Watson et al. 2006). Such a column density implies a very strong extinction of the optical AG and, consequently, an extreme chromaticity: more than 10-magnitude extinction in the V band (Zombeck 1990) and more than 30 magnitudes at 1800 Å. Indeed, the optical AG was very dim (a fitted spectral index, -0.33 , between the X-band and the optical band, compared to -0.8 to -1.1 in ‘normal’ GRBs. In fact, according to Jakobson et al. (2004), GRB 050401 qualified as a ‘dark burst’. It would not

be a good case to discuss (unattenuated) chromaticity, or the lack thereof.

GRB 070508. Swift’s XRT started to measure the X-ray light curve of this GRB 82s after the GRB trigger. Even at this early time, it already displays the shallow-decay plateau phase of a canonical AG, which later bends into a power-law decline, as shown in Fig. 3a.

GRB 060813, shown in Fig. 3b, is a case in which the prompt radiation is not seen by the XRT, and the AG has no obvious flares. In spite of some evidence for local variability, the smoothly bending AG is well described by the CB model ($\chi^2/dof = 1.07$ for 254 *dof*). Had the break happened a bit earlier, as in other cases, the X-ray AG would look like a power-law. The last data point lies below the fit, it could be due to an overestimated background.

GRB 060418, whose achromatic AG was studied in detail by Molinari et al. (2007). Its X-ray AG evolves fast into a power-law decline, see Fig. 3c. The CB-model fit returns an early break at $t_b = 123$ s, well hidden under the flaring activity during the fast-decline phase of the prompt emission. The transition from an ICS-dominated regime to one in which SR is prevalent is corroborated by the fast spectral softening of the tail of the flare from around $t \sim 130$ s (Evans et al. 2007), which suddenly turns, at $t \sim 165$ s, into the much harder time-independent power-law spectrum characteristic of the synchrotron AG (DDD2007b). We have checked that the reasonable $\chi^2/dof = 1.21$ for 295 *dof* of the fit shown in the figure can be reduced to $\chi^2/dof \sim 1$ by including X-ray flares between 5 to 10 ks, or by replacing the fluctuating data points by average values.

GRB 050717, studied in detail by Krimm et al. (2006). It had the largest inferred peak energy of all Swift GRBs, $E_p = 2401(-568/+781)$ keV, despite its estimated large redshift, $z > 2.7$. At this z -limit, $E_{\text{iso}} \sim 1.1 \times 10^{54}$ erg, and the local peak energy is $(1+z)E_p \sim 8840$ keV. It also had an initially very bright X-ray AG, after the fast declining prompt emission, with a power-law decline from $t \sim 200$ s onwards. The fit in Fig. 3d returns an early break-time limit, $t_b < 55$ s, well hidden under the prompt-emission tail. The CB-model interpretation of the transition from a prompt ICS radiation to a synchrotron AG is supported by the observed rapid spectral softening of the tail of the prompt emission and its sudden change at $t \sim 200$ s into the harder time-independent power-law spectrum of the synchrotron AG (DDD2007b). In the case of this GRB the best-fit value, $p = 1.67$, does not satisfy Eq. (8), with $\Gamma = 1.61 \pm 0.10$, as inferred from the X-ray spectrum with a fixed column density limited to the Galactic one (Krimm et al. 2006). However, $p = 1.67$ is consistent with $\Gamma = 1.88 \pm 0.15$ of the AG for $t > 200$ s, the spectral index reported by Zhang et al. (2007), after inclusion of host-galaxy and IGM absorption.

GRB 061126, studied in detail by Perley et al. (2008) had two major prompt pulses. Due to an Earth-limb constraint, Swift slewed to the burst’s direction only 23 minutes after

its localization by its Burst Alert Telescope (BAT). Its light curve, measured by the XRT between 1.6 ks and 1.88 Ms, is shown in Fig. 4a. The X-ray light curve was reported to be well fit by a power-law in time with index 1.29 ± 0.08 (Sbarufatti et al. 2006). A CB-model fit, with $p = 1.89$ and $t_b < 104$ s, is shown in Fig. 4a. There is a possible indication in the data of a steeper decay between 1.6 ks and 3.6 ks, which might belong to the tail of another CB with a smaller t_b . Cases of AGs clearly requiring two CBs will be discussed anon.

GRB 071025. Swift’s XRT started observations of the X-ray light curve 146s after the BAT trigger. The initial relatively hard spectrum ($\Gamma = 1.4$) softened beyond 300s and the light curve declined like a single power-law, consistent with the CB-model’s asymptotic power-law decline with a power-law index $\simeq 1.6$, as shown in Fig. 4b. The data suggest a flaring activity between 4 ks and 40 ks. The effect of such flares on the CB-model X-ray light curve is illustrated in the figure by adding an ICS flare around 40 ks with parameters (peak time, width and normalization) chosen, as in all other cases with clear flares, to best fit the data.

GRB 070125, studied in detail by Bellm et al. (2007). It was detected by Mars Odyssey, Suzaku, INTEGRAL, and RHESSI. It is one of the Swift-era GRBs with the largest measured values of $E_{\text{iso}} \sim 1 \times 10^{54}$ erg, $L_p \sim 3 \times 10^{53}$ erg s $^{-1}$, and source-frame $(1+z)E_p \sim 1100$ keV. The initial detection of this GRB occurred while it was not in the BAT field of view during the beginning of the prompt emission, and its XRT light curve starts at 46 ks after the burst. As shown in Fig. 4c its power-law decline is well described by the CB model. The feature at ~ 110 ks can be interpreted as an X-ray flare, as in the figure.

GRB 061007, whose AG was studied in detail by Schady et al. (2006) and Mundell et al. (2007), was the brightest GRB detected by Swift and was accompanied by an exceptionally luminous X-ray and UV/optical afterglow, which decayed as a power law with an index 1.65 ± 0.02 . It had the largest values of $E_{\text{iso}} \sim 1 \times 10^{54}$ erg, $L_p \sim 2 \times 10^{53}$ erg s $^{-1}$ and an emission-point peak energy, $(1+z)E_p \sim 1000$ keV (Golenetskii et al. 2006). This GRB is the best example to date of a bright X-ray AG, well-sampled from the start of the XRT observations (86s after the BAT trigger) to 10^6 s. The AG, shown in Fig. 4d, is power-law behaved right after the tail of the prompt emission. The CB-model fit returns $t_b < 89$ s, below which the χ^2/dof (a reasonable 1.13 for 1030 *dof*) stays put.

GRB 071020, measured by Swift’s XRT between 68s and 1.7 Ms after trigger, and shown in Fig. 5b. Holland et al. (2007) fitted the data with a broken power-law with an initial decay index of ≈ 0.5 , a break at $t_b = 160$ s, and a late-time decay index of 1.14 ± 0.02 . The fit is poor between 1.5 ks and 1.5 Ms. A CB-model fit with a single CB is also unsatisfactory. The addition of a second CB to the AG’s description, as in the fit shown in Fig. 5a, greatly improves the fit to $\chi^2/dof = 1.52$ for 174 *dof*, acceptable in view of what appears to be evidence for flaring activity, from 1.5 to 15 ks, which we have not endeavoured to describe,

given the scarcity of data.

XRF 050416A. The complex X-ray light curve of this XRF was monitored up to 74 days after the burst (Mangano et al. 2007). The late decline rate of the light curve is significantly slower than expected in the CB model from the observed photon spectral index Γ , namely $t^{-\Gamma-1/2} \sim t^{-1.5 \pm 0.10}$. The prompt signal of XRF 050416A had two clear pulses which, in the CB model, correspond to two separate CBs. The X-ray light curve, modeled with two CBs and shown in Fig. 5b, has a SR-component late-power decay that –although it is not readable ‘by eye’ due to the late-occurring ICS flare– is compatible with the predicted one.

GRB 060105, whose X-ray light curve was studied in detail by Tashiro et al. (2007). Following the prompt emission, which ended with a very steep decay, the light curve is canonical, it has a shallow decay after 180s and steepens at around 500s to a fast power-law decline, with a weak flaring activity superposed on it. The deviations from a smooth X-ray light curve may be caused by the flaring activity, not included in this particular fit, whose $\chi^2/dof = 1.36$ for 854 *dof*, is not inadequate.

GRB 060607A, was studied by Molinari et al. (2007). Its complex X-ray light curve, like that of quite a few other GRBs, is dominated by strong flaring activity, as can be seen in Fig. 5d, with its many flares superimposed on the AG of a fitted, single, dominant CB. This fit, which can be improved by splitting the last flare into two, is a very rough description ($\chi^2/dof = 4.9$ for 440 *dof*), not a proof of the quality of a prediction. Moreover, in cases with such a prominent flaring activity, the photon spectral index of the AG data is an average between the typical index of flares, $\Gamma = 1$, and that of synchrotron AG, $\Gamma = 2$, i.e., an average significantly smaller than that of the synchrotron AG. Thus, we do not expect such a labyrinthine AG to satisfy the CB-model spectral-index relations, Eqs. (6,8).

The afterglow as a function of time and frequency

We have summarized in Eq. (4) the predicted form of the spectral energy density of the AG of a GRB, in which the time-dependence and the energy-dependence are explicitly concatenated. In the large-frequency limit of the X-ray domain, the expression simplifies to that of Eq. (6), implying a predicted relation between the temporal index p (which we fit to the XRT light curve of the X-ray AG) and the spectral index Γ , independently fitted by the Swift team to the X-ray AG spectrum after correcting for attenuation, and reported by Zhang et al. (2007). The prediction is particularly simple, and is most transparently readable in the late- t limit for the AGs’ dependence on t and ν , Eq. (8), in which both the time and the frequency functional forms are separate power laws.

The values of p and Γ are listed in Table 1. Notice that Γ varies over a significant range of central values, 1.61 to 2.25, and that the measurements are not compatible within errors with a common value. To illustrate the prediction in Eqs. (6,8), we have plotted in Fig. 6 the ratio $r = p/(2\Gamma - 2)$ (predicted to be unity) for the various GRBs analyzed in this paper, and added a few other analyzed in the same fashion. The results are quite satisfactory. The mean value of r , for instance, is 0.999 ± 0.025 for the GRBs analyzed here, 1.000 ± 0.019 for the ensemble plotted in Fig. 6.

The (t_b, E_{iso}) and (t_b, E_p) correlations

In the CB model, the functional dependence on θ and γ_0 of the deceleration-bend time of the synchrotron AG, t_b , as well as its normalization, are specified by Eq. (7). This is also the case for the parameters, E_p and E_{iso} of Eqs. (9) and (10), of the prompt ICS signal. As we saw in the introduction, this implies explicit correlations between t_b and the prompt observables. The (t_b, E_{iso}) correlation is illustrated in Fig. 1b for various choices of θ and γ_0 , with the rest of the parameters in t_b and E_{iso} fixed to reference values in Eqs. (7,10).

In Fig. 7 we plot, in the $[t_b/(1+z), E_{\text{iso}}]$ plane, the values returned by our analysis of the GRBs we have discussed, see Table 1. The GRBs represented by arrows reflect the fact that some data are just upper limits. The large shaded contour plot in the figure is the boundary of the domain covered by letting γ_0 vary from 500 to 1500, θ from 0 to 8 mrad, typical ranges encountered in the CB-model analysis of GRBs. Moreover, the normalization of t_b in Eq. (7) was varied from its central value in Eq. (7) to 1/2 order of magnitude above it, and the normalization of E_{iso} in Eq. (10) from its central value to 1/2 order of magnitude below and above it. The variability in these normalizations is best ascertained by the current analysis, it has been chosen to make Fig. 7 ‘look good’. We have added to the figure the results for a few GRBs which we have previously analyzed along the same lines in DDD2007a,b.

There is no reason to expect the data to populate uniformly the region bounded by the contour in Fig. 7. On the contrary. The relativistically beamed radiation from a point in a CB initially subtends an angle $1/\gamma_0$. Observers at an angle θ from the axial direction have a chance $\propto \theta d\theta$ of being illuminated. At $\theta > 1/\gamma_0$ this chance decreases abruptly, given the fast fall of the Doppler factor. All in all, $\theta \sim 1/\gamma_0$ is the optimal observation angle, for *any* γ_0 . Most GRBs, then, should be seen at $\theta \gamma_0 = \mathcal{O}(1)$. The thick straight line in Fig. 7 is $t_b(E_{\text{iso}})$ at fixed $\theta \gamma_0$, for which $t_b/(1+z) \propto \gamma_0^{-3}$ and $E_{\text{iso}} \propto \delta_0^3 \propto \gamma_0^3$. Thus:

$$t_b/(1+z) \propto E_{\text{iso}}^{-1}. \quad (11)$$

The data follow this trend well, but at the high- E_{iso} end, at which they bend as in Fig. 1b.

In Fig. 8 we plot, in the $[t_b/(1+z), (1+z)E_p]$ plane, the corresponding results of our analysis. The shaded domain is obtained with the same ranges in γ_0, θ –and in the normalization of t_b – as in the previous paragraph. The normalization of E_p has been allowed to vary from 1/3 to 1/6 of its value in Eq. (9)⁵. The points plotted as ellipses have an unknown z , which we have let vary from 0 to 2.75, the average for Swift-era GRBs (Greiner, <http://www.mpe.mpg.de/jcg/grbgen.html>). At fixed θ, γ_0 , $(1+z)E_p \propto \gamma_0 \delta_0 \propto \gamma_0^2$, so that:

$$t_b/(1+z) \propto [(1+z)E_p]^{-3/2}. \quad (12)$$

The rest of the comments are as in the discussion of the (t_b, E_{iso}) correlation.

Another direct way to ascertain the variability of the parameters governing the normalizations of E_p and E_{iso} is to study their scatter plot (DD2000b, Amati et al. 2002, DD2004, DDD2007c, Amati 2006) for a large collection of GRBs and XRFs. This is done in Fig. 9, where the varying-power correlation predicted by the CB model (DDD2007c) is shown, and to which the GRBs with known z , E_p and E_{iso} , among those studied here, are added. The figure shows that a total uncertainty of a factor of 2 in the norm of E_p and of one an order of magnitude in the norm of E_{iso} (as we have adopted) is adequate to bracket the data.

We have also tested elsewhere (DDD2007d) the correlation, apparent in Fig. 1a, between t_b and the normalization of the AG. Willingale et al. (2007) and Nava et al. (2006) had collected and analyzed a large set of GRBs, and made a scatter plot of t_b versus the total AG energy in the 15-150 keV X-ray band up to time t_b . To use this available information, we studied this correlation in its Willingale-Nava form. Like the ones in Figs. 7 and 8, it turns out to follow the pattern expected in the CB model.

The correlations between t_b and E_{iso} or E_p demonstrate that ‘sub-energetic’ GRBs (or XRFs) have large ‘break’ times and, consequently, easily observable ‘breaks’. As GRBs become more ‘energetic’, t_b decreases and the chances increase to ‘miss the break’, which may be hidden under the prompt radiation, or may precede the Swift slew-time minimum, or the start of the observations.

⁵The E_p of Eq. (9) is the peak energy at the start of a pulse; set it to $t=0$. The energy of the radiation is predicted to decrease during the pulse’s duration: $E_p(t) \approx E_p(0) [1 - t/(\Delta^2 + t^2)^{1/2}]$, with Δ the width parameter (the full width at half-maximum, FWHM, is $\sim 1.8 \Delta$). Observers usually report E_p at the peak’s maximum, expected to be $E_p(t_{\text{max}}) \approx 0.23 E_p(0)$, or its pulse-averaged value: $\langle E_p \rangle \approx 0.18 E_p(0)$ over the FWHM. We have not corrected for these facts, which may explain the choice of the ‘best’ domain.

6. Conclusions and outlook

A virtue of astrophysical X-ray data is that, in many instances and relative to lower-frequency bands, the corrections for attenuation are simpler and more reliable. The strength of Swift in dealing with transient phenomena is, as the satellite’s name reflects, the prompt start of its data-taking after an alert. This has made the Swift results an excellent testing ground for theories of GRBs and XRFs. In particular, the ability to monitor the X-ray flux over a very wide range of times has provided decisive tests of the theoretical predictions.

Filling the pre-Swift gap in the data –between ‘prompt’ and ‘afterglow’ radiations– has led to a better understanding of the mechanisms responsible for them. In the CB model they are different: inverse Compton scattering and synchrotron radiation, respectively. We have previously argued that the strong case for an ICS origin of the ‘prompt’ radiation (DD2004) has been reconfirmed by the analysis of the Swift X-ray flares, and the fast decay of the prompt signals (DDD2007b). In this respect the study of X-ray and optical data is also particularly meaningful (DDD2007a). The observed correlations between prompt observables — E_{iso} , E_p , L_p and pulse rise-time, lag-time and variability— also agree with the CB-model (see DDD2007c and references therein). These correlations follow from the same simple considerations, that we have emphasized in this paper, on the dependence of the cited prompt observables on the Lorentz and Doppler factors of the radiation emitted by a quasi-point-like relativistically moving source.

The CB-model’s expectations for the interplay between ICS and SR were confirmed by the analysis of the ‘canonical’ shape of many Swift X-ray light curves (DDD2007a). The extreme canonical case is still GRB 980425, shown in Fig. (2a). The trend of the ‘hardness ratios’ reflecting the spectral behaviour, and the spectral index itself, also corroborate the expected transitional behaviour (DDD2007b), as the dominant mechanism evolves from ICS to SR.

In this paper we have shown in detail how the variety of X-ray AG shapes, with and without ‘breaks’, is also to be expected from a decelerating jet of effectively pointlike cannonballs, as in Fig. (1a). That the AG emission mechanism is SR from CBs slowing down in the way approximated by Eq. (2) is confirmed by the detailed frequency and time-dependences of Eq. (4) for the spectral energy density. We have presented a study of the correlation between the synchrotron AGs’ t - and ν - dependences, specified in the X-ray domain by Eq. (6). This results in a relation between the AGs’ spectral index Γ , and the index p appearing in their time dependence, a very simple relation at the late times at which the time dependence is also a power-law, see Eq. (8). The prediction is tested in Fig. 6.

In the CB model, the understanding of AGs with breaks or no breaks turns out to

be clear: the ‘missing’ SR breaks are hiding under the prompt ICS radiation, or occur too early to be seen. This sounds like a trivial and model-independent excuse. It is not. It is supported by our case-by-case analysis of AG shapes. Moreover, a crucial ingredient — the angle of observation of the jet, compared to the beaming angle of its Doppler-boosted radiation— is validated by the correlations, e.g. the luminous AGs are the ones with early or even undetectable breaks, as in Fig. 1a, and as in many of the examples we discussed here (the correlation between t_b and the energy in the X-ray AG was studied in DDD2007d). Our conclusions are also supported by the correlations between the CBs’ deceleration-bend ‘break-times’, t_b (in the synchrotron AGs), and the values of E_{iso} and E_p (in the prompt Compton signal). These correlations, shown in Figs. 7 and 8, reconfirm the consistency of the overall picture.

We have given no comment in the conclusions to our fits to the GRBs and XRFs that we have studied. This is because the point we would like to make is *not* that the CB model can be used to fit the data very well. The main issue, in our view, is *how* a model, preferably in a predictive manner and in terms of very few concrete concepts –like its radiation mechanisms, the aperture of its jets and the angle from which they are viewed– can be used to understand the ensemble of long-duration GRBs, and XRFs⁶. After all, phenomena that require ever-increasingly complex explanations are of limited scientific interest.

REFERENCES

- Amati, L., Frontera, F., Tavani, M., et al. 2002, A&A, 390, 81
- Amati, L., 2006, MNRAS, 372, 233
- Bellm, E., et al. 2007, arXiv0710.4590
- Bhat, P. N., et al. 1992, Nature, 359, 217
- Burrows, D. N. & Racusin, J. 2007, arXiv: astro-ph/0702633
- Costa, E., et al. 1997, Nature, 387, 783
- Covino, S., et al. 2006, Nuovo Cim. B 121, 1171
- Dado, S. & Dar, A. 2005, Ap.J. 627, L109

⁶XRFs, we allege, are long-duration GRBs viewed at large angles, but what is a short-duration GRB? We are currently writing a paper on how the CB model may shed light on this question.

- Dado, S., Dar, A. & De Rújula, A. 2002, A&A, 388, 1079 (DDD2002)
- Dado, S., Dar, A. & De Rújula, A. 2003a, A&A, 401, 243 (DDD2003a)
- Dado, S., Dar, A. & De Rújula, A. 2004a, A&A, 422, 381 (DDD2004a)
- Dado S., Dar, A., & De Rújula, A., 2006, ApJ, 646, L21 (DDD2006)
- Dado, S., Dar, A. & De Rújula, A. 2007a, arXiv0706.0880 (DDD2007a)
- Dado, S., Dar, A. & De Rújula, A. 2007b, arXiv0709.4307 (DDD2007b)
- Dado, S., Dar, A. & De Rújula, A. 2007c, ApJ, 663, 400 (DDD2007c)
- Dado, S., Dar, A. & De Rújula, A. 2007d, astro-ph/0703700 (DDD2007d)
- Dar, A. 1997, *Very High Energy Phenomena in the Universe* (Editions Frontieres, Eds. Y. Giraud-Heraud and J. Tran Thanh Van,) p.69 (arXiv:astro-ph/9704187)
- Dar, A. 1998, ApJ, 500, L93
- Dar, A. & De Rújula, A. 2000a, arXiv: astro-ph/0008474 (DD2000a)
- Dar, A. & De Rújula, A. 2000b, arXiv: astro-ph/0012227 (DD2000b)
- Dar, A. & De Rújula, A. 2004, Physics Reports, 405, 203 (DD2004)
- Dar, A. & De Rújula, A. 2006, eprint arXiv: hep-ph/0606199 Submitted to Phys. Repts. (DD2006)
- Dar, A. & Plaga, R. 1999, A&A, 349, 259
- Dar, A., Kozlovsky, B., Nussinov, S., Ramaty, R. 1992, ApJ, 388, 164
- De Pasquale, M., et al. 2006, MNRAS 365, 1031
- De Rújula, A. 1987, Phys. Lett. 193, 514
- De Rújula, A. 2007, arXiv0711.0970
- Evans, P. A., et al. 2007, arXiv: astro-ph/0704.0128
- Frederiksen, J. K., et al. 2004, ApJ, 608, L13
- Frail, D. A., et al. 2001, ApJ, 562, L55
- Ghisellini, G., Celotti, A., Lazzati, D. 2000, MNRAS, 313, L1

- Golenetskii, S., et al. 2006, GCN 5722
- Goodman, J. 1986, ApJ, 308, L47
- Goodman, J., Dar, A. & Nussinov, S. 1987, ApJ, 314, L7
- Groot, P. J., et al. 1998, 493, L27
- Grupe, D., et al. 2007, ApJ, 662, 443
- Harrison, F. A., et al. 1999, ApJ, 523L, 121
- Holland, S., et al. 2007, GCN Report 94, 1
- Hurkett, C. P. et al. 2006, MNRAS, 368, 1101
- Jakobsson, P., et al. 2004, ApJ, 617, L21
- Kocevski, D. & Butler, N. 2007, arXiv0707.4478
- Kouveliotou, C., et al. 2004, ApJ, 608, 872
- Krimm, H. A., et al. 2006, ApJ. 648, 1117
- Liang, E. W., et al. 2007, ApJ, 653, L81
- Mangano, V., et al. 2007, ApJ, 654, 403
- Meegan, C. A. et al. 1992, Nature, 355, 143
- Mészáros, P. & Rees, M. J. 1997, ApJ, 476, 232
- Mészáros, P. 2002, ARA&A, 40, 137
- Metzger, M. R., et al. 1997, Nature, 387, 878
- Molinari, E., et al. 2007, A&A, 13, 469L
- Mundell, C. G., et al. 2007, ApJ, 660, 489
- Nava, L., et al. 2006, A&A, 450, 471
- Paczynski, B. 1986, ApJ, 308, L43
- Panaitescu, A., et al. 2006, MNRAS, 369, 2059
- Perley, D. A., et al. 2008, ApJ, 672, 449

- Pian, E., et al. 2000, *ApJ*, 536, 778
- Piran, T. 1999, *Physics Reports*, 314, 575
- Piran, T. 2000, *Physics Reports*, 333, 529
- Rees, M. J., & Meszaros, P. 1992, *MNRAS*, 258, 41P
- Rhoads, J. E. 1997, *ApJ*, 487, L1
- Rhoads, J. E. 1999, *ApJ*, 525, 737
- Sahu, K. C., et al. 1997, *Nature*, 387, 476
- Sari, R., Piran, T. & Halpern, J. P. 1999, *ApJ*, 519, L17
- Sbarufatti, B., et al. 2006, *GCN Circ.* 5862
- Shady, P., et al. 2006, *astro-ph/0611081*
- Schaefer, B. E. 2007, *ApJ*, 660, 16
- Shaviv, N. J. & Dar, A. 1995, *ApJ*, 447, 863
- Stanek, K. Z., et al. 1999, *ApJ*, 522L, 39
- Tashiro, M. S., et al. 2006, *PASJ*, 59, 361
- van Paradijs, J., et al. 1997, *Nature*, 386, 686
- Watson, D., et al. 2006, *ApJ*, 652, 1011
- Willingale, R., O’Brien, P. T., Osborne, J. P., Godet, et al. *astro-ph/0612031*
- Woosley, S. E. 1993, *ApJ*, 405, 273
- Zhang, B. B., Liang, E. W. & Zhang, B. 2007, *ApJ*, 666,1002
- Zombeck, M. 1990, *Handbook of Astrophys.* Ed. Cambridge Univ. Press

Table 1. GRB observables and CB-model best-fit afterglow parameters.

GRB	z	E_p	E_{iso}	Γ	p	$\gamma_0 \theta$	$t_b[\text{s}]$	$t_s[\text{s}]$	χ^2/dof
980425	0.0085	56	6.9 E47	$2.1 \pm ?$	2.20	9.17	145000	36000	31/0
060729	0.54	—	< 7 E51	2.10 ± 0.15	2.20	2.51	8300	130	1966/207
050505	4.27	214	—	1.90 ± 0.20	2.22	1.57	1980	2833	114/95
050401	2.90	132	3.5 E53	2.18 ± 0.10	2.20	0.80	1660	133	353/299
070508	0.82 ?	188	7.0 E52	2.05 ± 0.04	2.12	1.22	260	82	610/469
060813	—	214	—	1.98 ± 0.18	1.70	1.13	190	85	256/239
060418	1.49	230	9 E52	2.03 ± 0.04	2.20	1.73	123	84	339/280
050717	> 2.7 ?	2401	> 1 E54	1.61 ± 0.10	1.67	(0.08)	< 55	91	114/78
061126	1.159	620	1.1 E53	1.93 ± 0.12	1.89	(1.87)	< 104	1604	506/261
071025	—	—	—	—	2.20	(0.90)	< 68	150	330/243
070125	1.547	440	9.4 E53	2.10 ± 0.28	2.38	(1.19)	< 8060	47000	28/28
061007	1.261	498	1.0 E54	2.10 ± 0.20	2.26	(0.05)	< 89	86	1147/1015
071020	2.145	322	8.0 E52	1.86 ± 0.06	1.86	0.67	90	68	234/154
”					1.86	1.43	15100	68	
050416A	0.6535	15	1.2 E51	2.04 ± 0.11	2.00	1.05	944	85	101/92
”						2.00	14800	85	
060105	—	424	—	2.25 ± 0.10	2.33	0.53	510	96	1879/839
060607A	3.082	—	—	—	2.20	0.97	164	73	1119/404

The values of the peak energy, E_p (in keV) and E_{iso} (in erg) of the GRBs are from GCN reports of data of Konus-Wind, RHESSI and Suzaku. The GRB redshifts are from GCN reports from ground-based optical telescopes. The start times t_s , of the XRT data after the BAT trigger, are from the Swift repository (Evans et al. 2007). The unabsorbed spectral indices Γ are from Swift GCN reports and Zhang, Liang & Zhang (2007). The CB-model fits return p , $\gamma_0 \theta$ and t_b . The parenthesized $\gamma_0 \theta$ are for t_b at its upper limit.

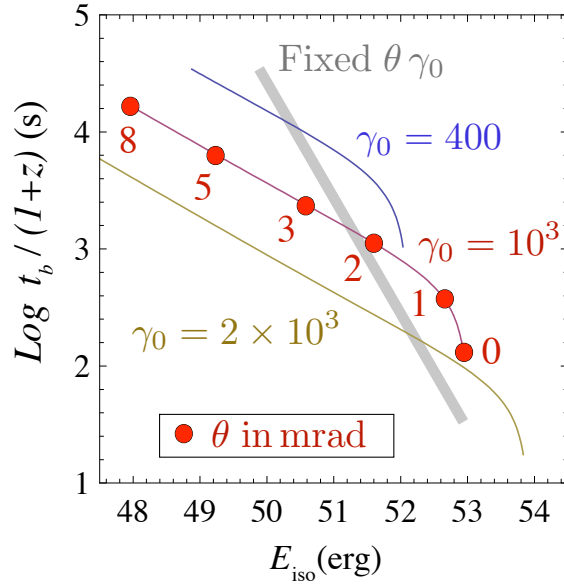
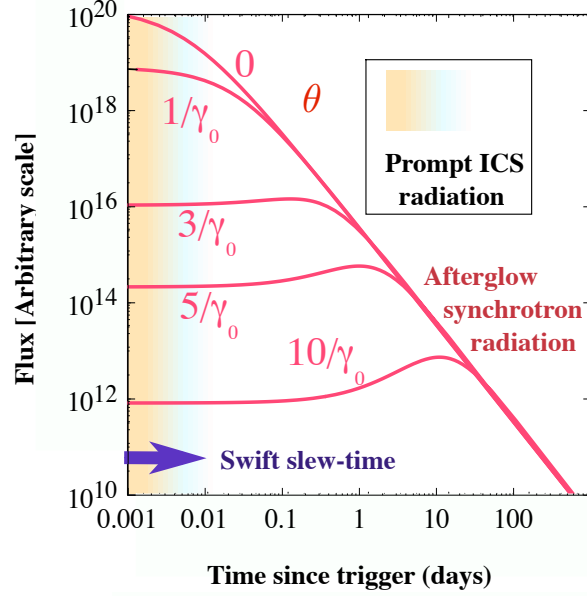


Fig. 1.— **Top: (a)** Dependence of the synchrotron AG on θ , for $\gamma_0 = 10^3$ (DDD2002), with nR^2/N_B as in Eq. (7), and a shaded domain for a typical time-zone of prompt-radiation dominance. **Bottom: (b)** Correlation between the ‘break-time’, $t_b/(1+z)$, of the AG and the isotropic energy, E_{iso} , of the prompt radiation, for typical parameters and various values of γ_0 . The dots along the $\gamma_0 = 10^3$ line are labeled with values of θ in mrad. The predicted fast drop of the curves at $\theta < 1$ mrad is due to the CBs not being precisely point-like (DDD2007d). The thick line is the correlation at $\theta \sim 1/\gamma_0$, the most probable observer’s angle.

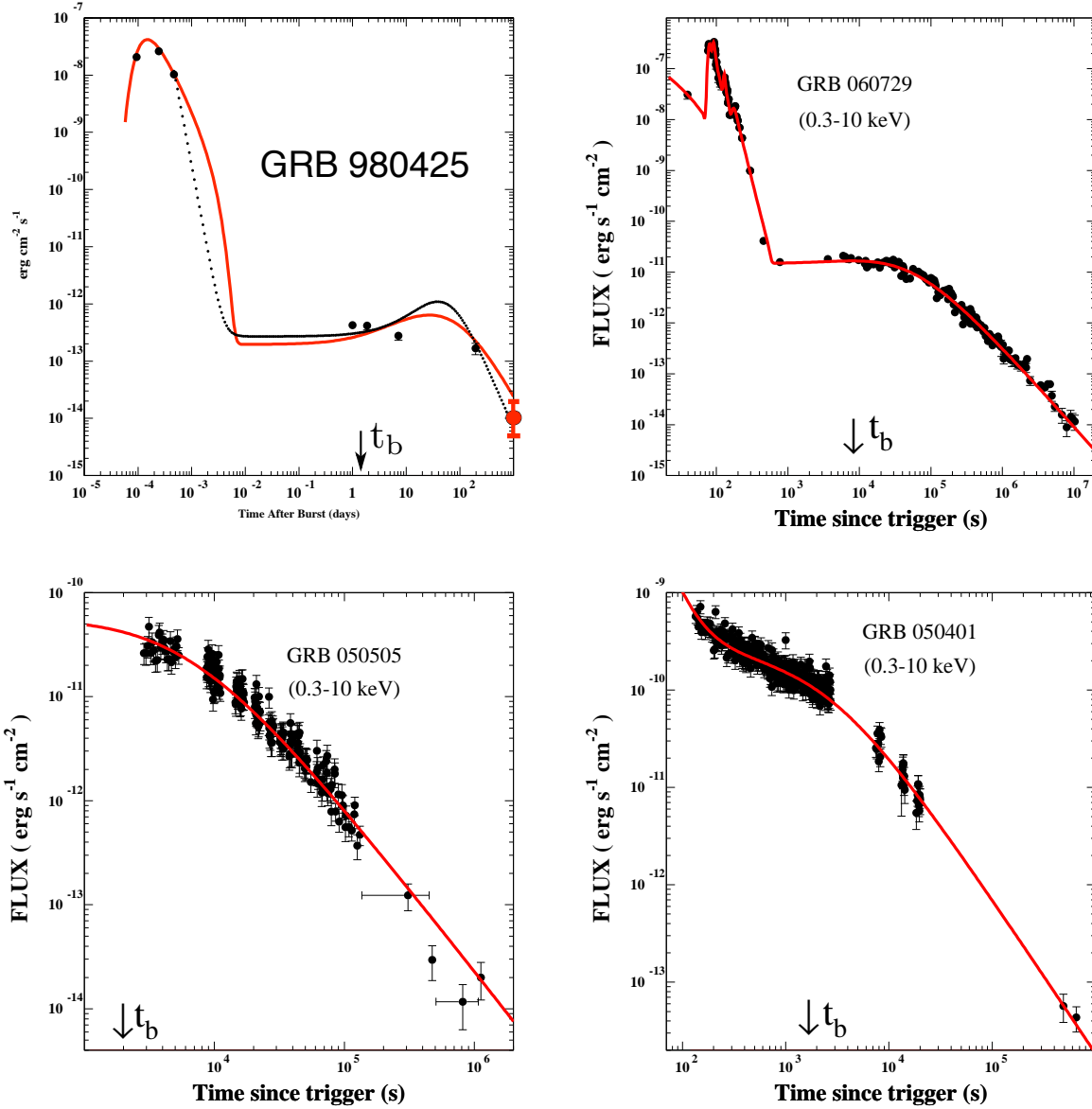


Fig. 2.— Comparison between the observed X-ray light curves of selected GRBs and their CB model fit: **Top left (a)**: GRB 980425. The last point was measured 1285 days after burst (Kouveliotou, et al. 2004). Dotted line: DDD2002. Continuous line: fit here as all other light curves. **Top right (b)**: GRB 060729. **Bottom left (c)**: GRB 050505. **Bottom right (d)**: GRB 050401. All light-curve data, but for GRB 980425, are from the Swift/XRT light curve repository (Evans et al. 2007).

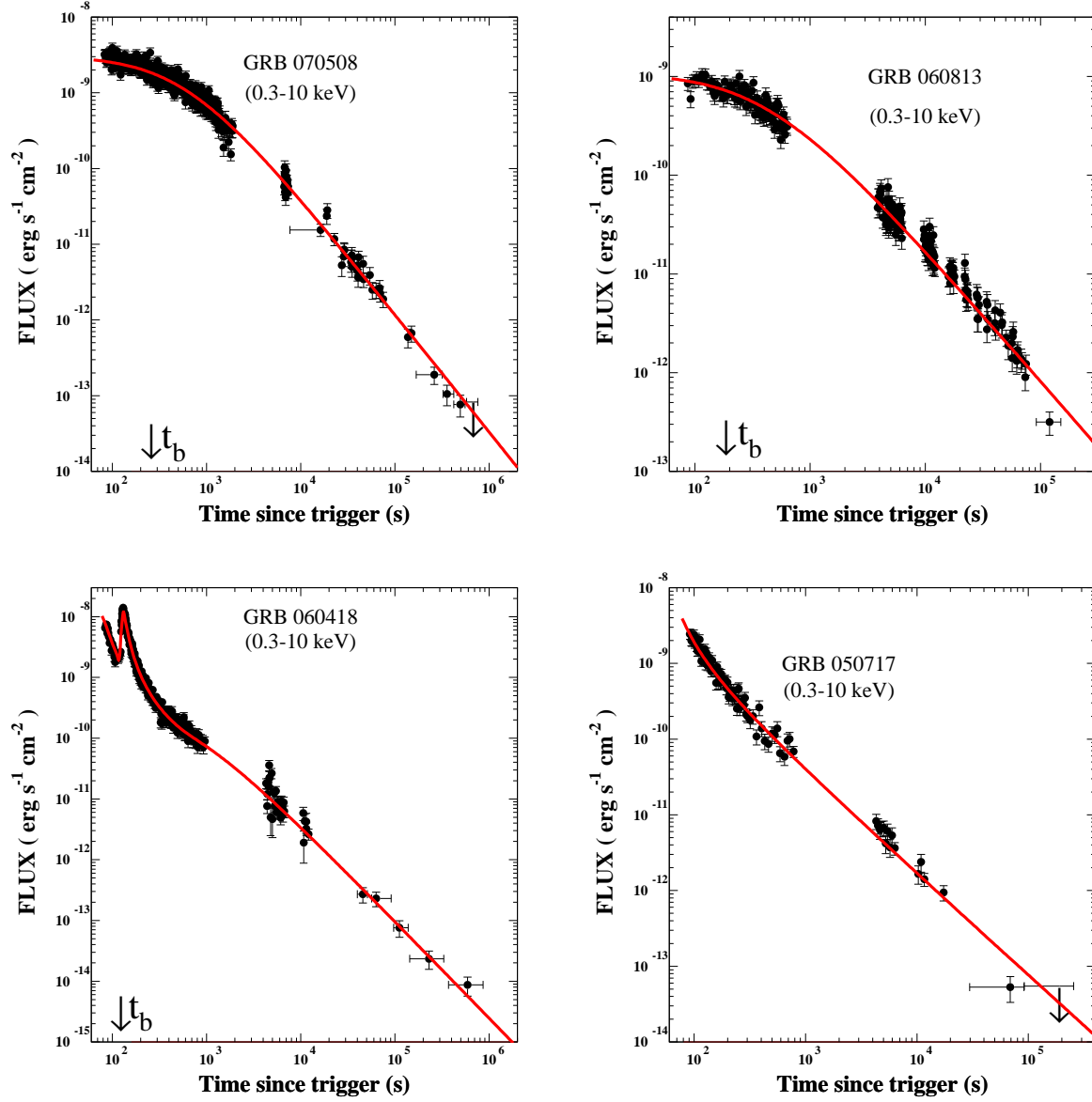


Fig. 3.— Comparison between the observed X-ray light curves of selected GRBs and their CB model fit: **Top left (a):** GRB 070508. **Top right (b):** GRB 060813. **Bottom left (c):** GRB 060418. **Bottom right (d):** GRB 050717. The light-curve data are from the Swift/XRT light curve repository (Evans et al. 2007).

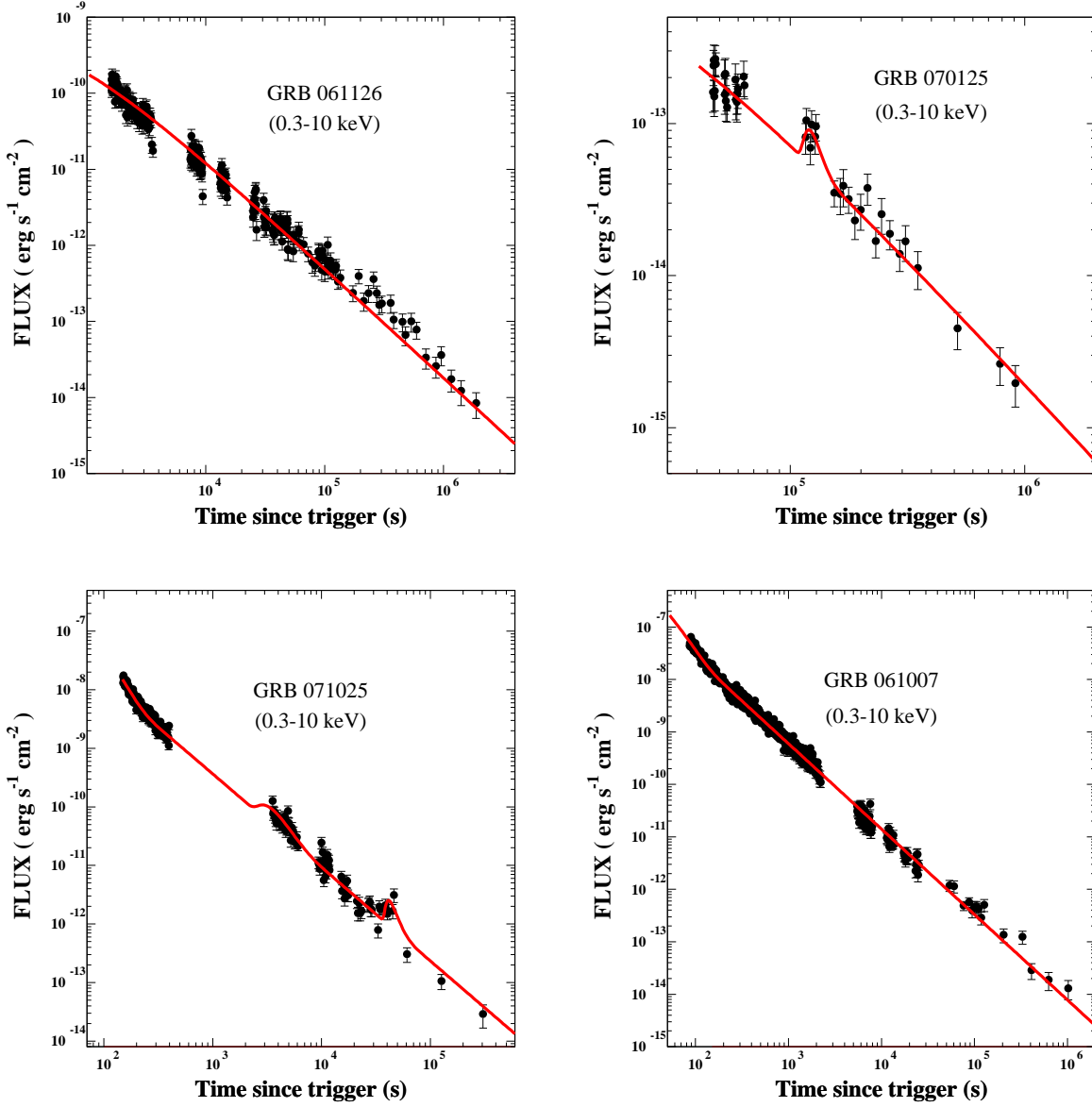


Fig. 4.— Comparison between the observed X-ray light curves of selected GRBs and their CB model fit: **Top left (a):** GRB 061126. **Top right (b):** GRB 070125. **Bottom left (c):** GRB 071025. **Bottom right (d):** GRB 061007. The light-curve data are from the Swift/XRT light curve repository (Evans et al. 2007).

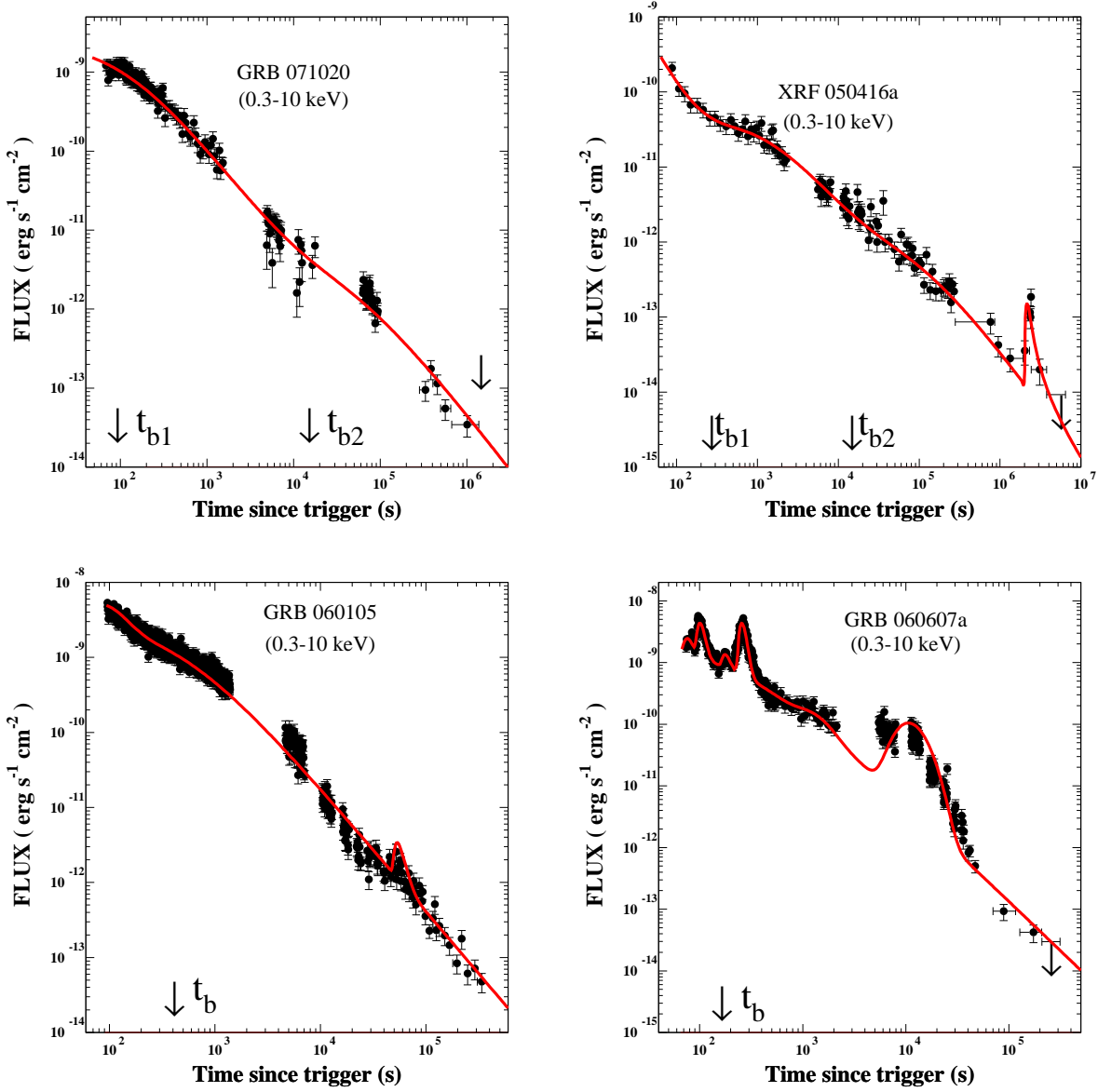


Fig. 5.— Comparison between the observed X-ray light curves of selected GRBs and their CB model fit: **Top left (a):** GRB 071020. **Top right (b):** GRB 050416A. **Bottom left (c):** GRB 060105. **Bottom right (d):** GRB 060607A. The light-curve data are from the Swift/XRT light curve repository (Evans et al. 2007).

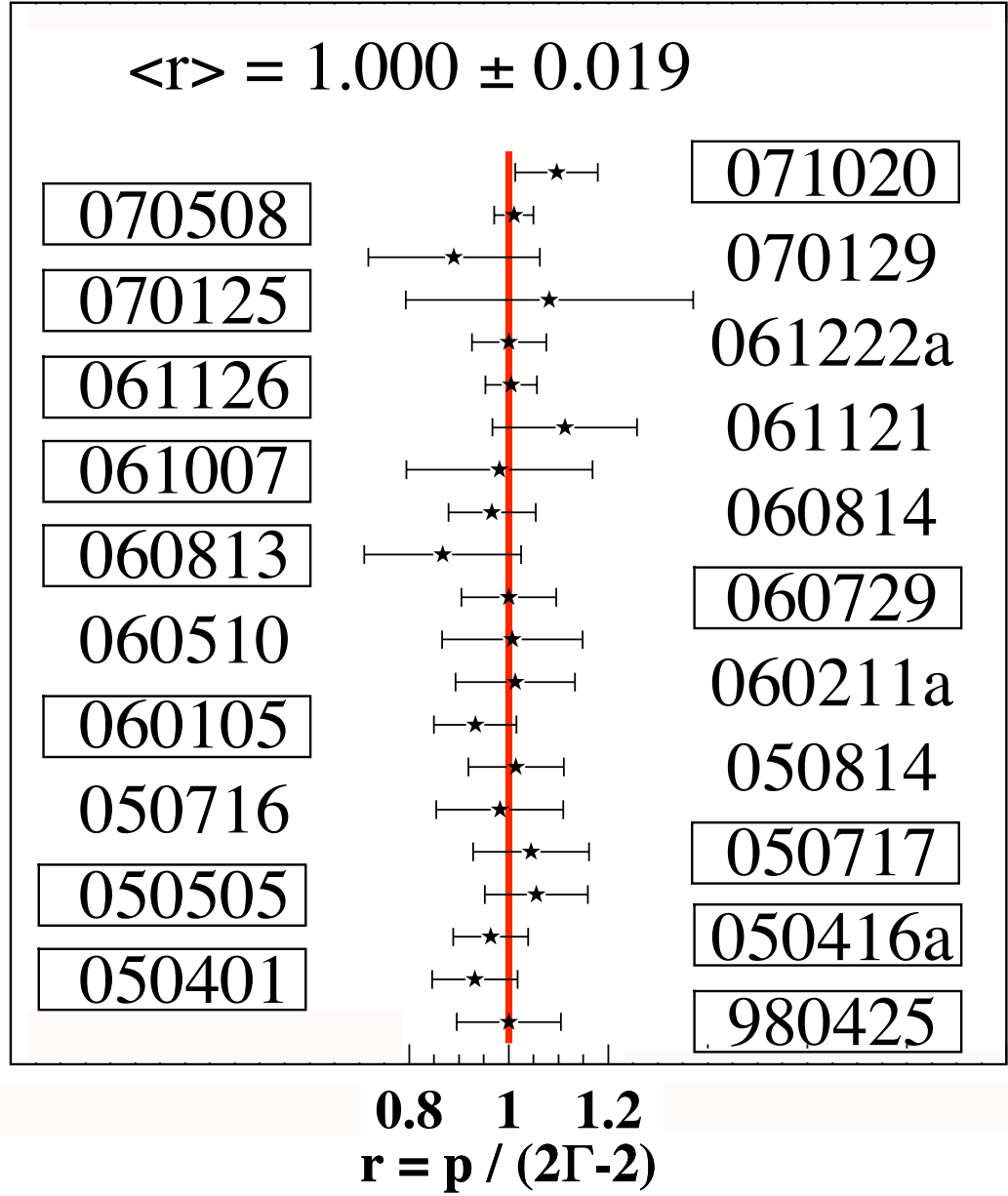


Fig. 6.— Test of the prediction, $r \equiv p / (2\Gamma - 2) = 1$, of Eq. (8), relating the temporal index, p , to the spectral one, Γ , of the afterglows of GRBs. The GRBs discussed in this paper are the outlined ones. We have extended this test to other GRBs analyzed in the same fashion.

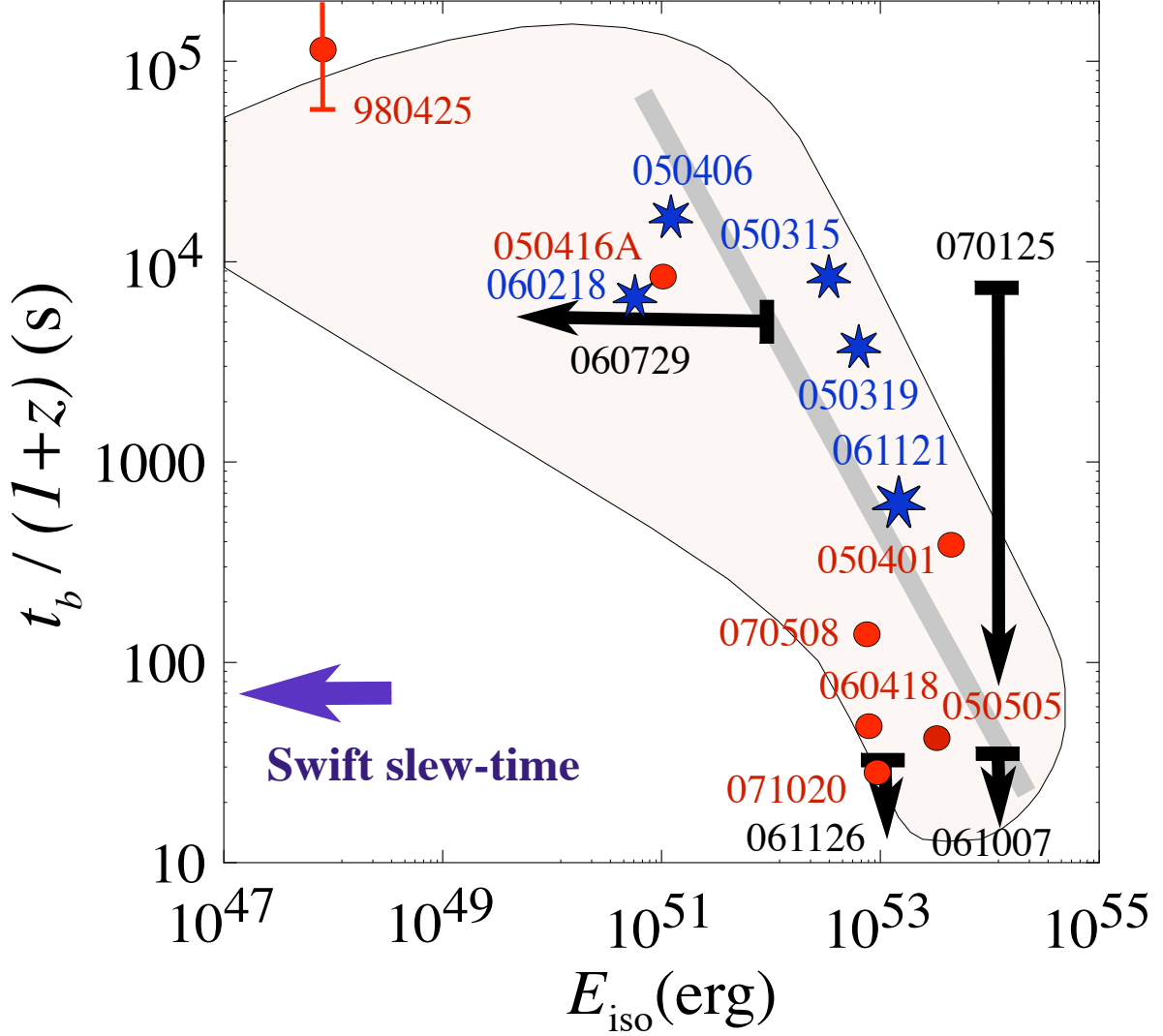


Fig. 7.— The $[t_b/(1+z), E_{iso}]$ correlation. The (red) circles are the GRBs of known E_{iso} analyzed in this paper, most of which have comparatively small t_b . The arrows reflect results for which only an upper limit is available. The (blue) stars are GRBs, mainly with ‘canonical’ X-ray light curves, analyzed in DDD2007a. The large shaded domain is the contour of a region obtained by letting the parameters vary as specified in the text. The shaded straight line is the expectation for GRBs viewed close to the most probable angle of observation, $\theta_{\gamma_0} = 1$.

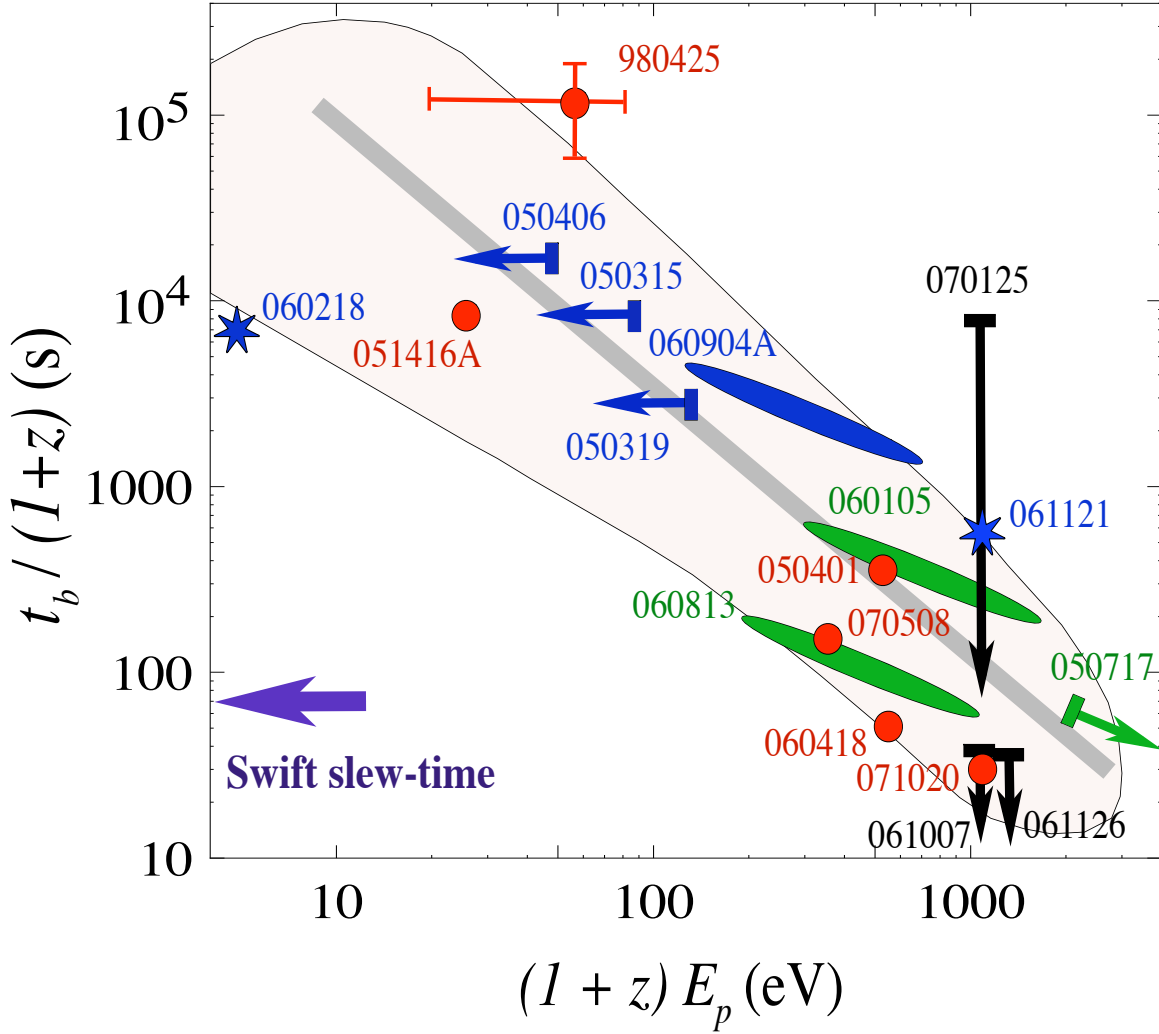


Fig. 8.— The $[t_b/(1+z), E_p]$ correlation. The (red) circles are the GRBs of known E_p analyzed in this paper, most of which have comparatively small t_b . The arrows reflect results for which only an upper limit is available. The ellipses are for GRBs of unknown z . The results that are not (red) circles or vertical arrows are GRBs, mainly with ‘canonical’ X-ray light curves, analyzed in DDD2007a. The large shaded domain is the contour of a region obtained by letting the parameters vary as specified in the text. The shaded straight line is the expectation for GRBs viewed close to the most probable angle of observation, $\theta_{\gamma_0} = 1$. The ‘true’ E_p of GRB 980425 could be smaller than reflected in this plot (Dado & Dar 2005).

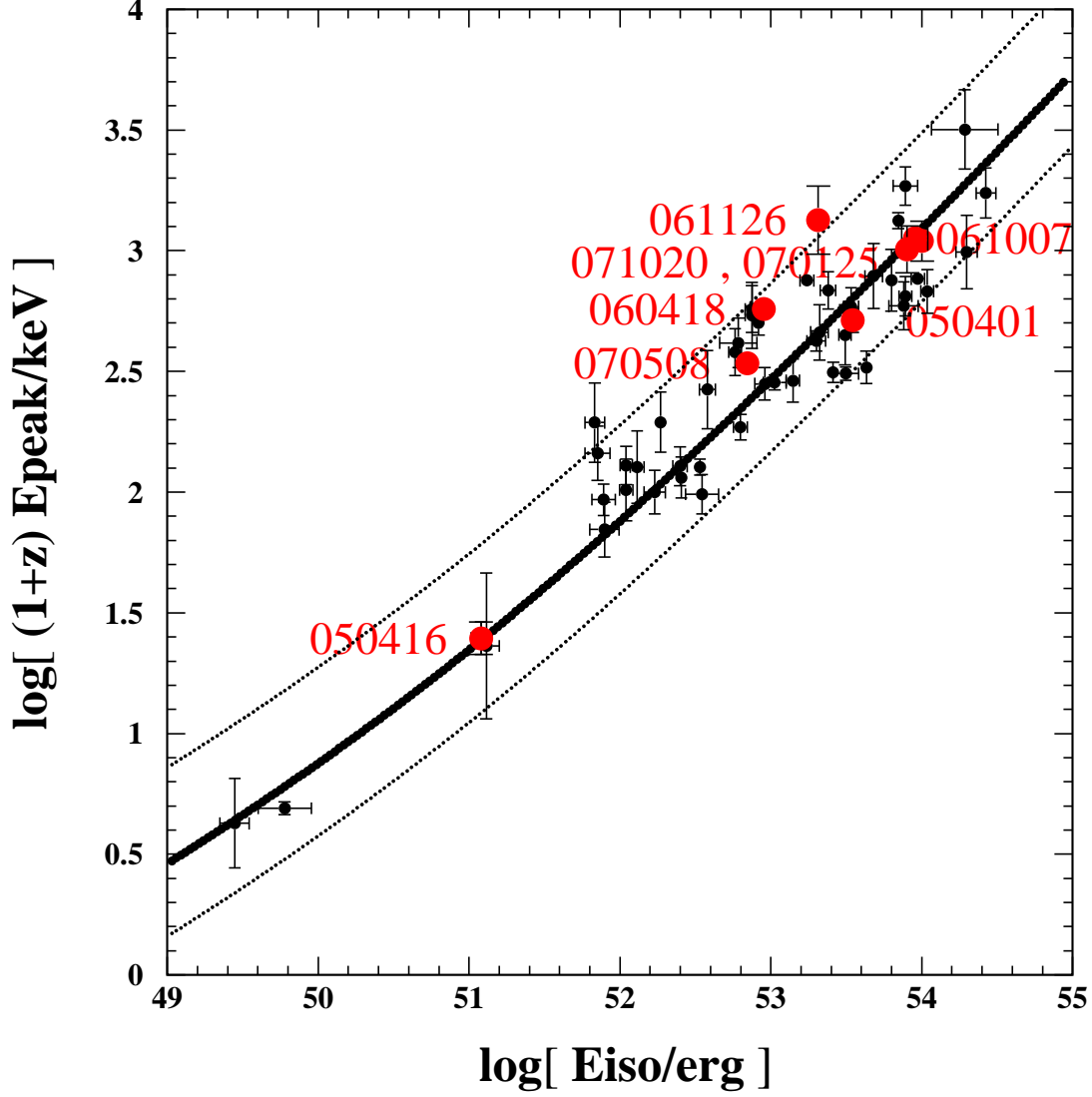


Fig. 9.— The $[(1+z) E_p, E_{\text{iso}}]$ correlation (DD2000b, Amati et al. 2002) for an ensemble of GRBs of known z , analyzed by Schaefer (2007). The central line is the CB-model's expectation (DDD2007c), the dotted lines bracket the observed case-by-case variability. The large (red) circles are the GRBs discussed in this paper which have known z , E_p and E_{iso} .